NOTES AND CORRESPONDENCE

Preliminary Tests of an Ultrasonic Thermoanemometer for Aircraft Measurements

A. MARILLIER, M. CABANE AND D. CRUETTE

Laboratoire de Météorologie, Université Pierre et Marie Curie, Paris

5 January 1990 and 25 January 1991

ABSTRACT

A prototype of an ultrasonic thermoanemometer, specially designed for aircraft measurements, has been developed. By measuring the transit time of ultrasonic pulses, one can deduce the speed of sound and then the air temperature (or the aircraft speed) at hundredth of a second intervals. In order to avoid the problems inherent to vibrations and to reduce the number of measurement paths, the flow has been channeled so as to be unidirectionnal. Wind tunnel studies allowed us to define a convenient geometry. Preliminary flight tests (up to 200 km h^{-1}) have been conducted.

1. Introduction

Atmospheric physics requires accurate measurement of air temperature outside and inside clouds. Most aircraft measurements of temperature are based upon the change in resistance as a function of temperature in a probe (such as a platinum wire or thermistor). After calibration the local temperature is obtained with a delay time that depends on the thermal inertia of the probe. Often the probes are operated to give a measurement every second, that is with a spatial resolution of a hundred (or more) meters. Furthermore, the airflow around the sensor produces a local heating that increases in proportion to the square of the aircraft velocity. For example, in the case of an airplane cruising at a speed of 400 km h^{-1} (111 m s^{-1}) at an altitude of 5000 m, the correction in temperature measurements is about 6°. This correction is often higher than temperature variations that are to be referenced. Moreover, when the aircraft penetrates a cloud, unless the probe is protected, droplets cover it with a liquid-water film. When the aircraft flies out of the cloud, water evaporation leads to a cooling of the probe and, for a period of time, the temperature indicated by the probe is lower than the real temperature. Even in the case of protected probes (reverse flow probes), Lawson and Cooper (1990) have shown that the probe gets wet in some warm clouds.

Here we propose the use of a well-known method that consists of measuring the velocity of an ultrasonic pulse and deducing the air temperature and aircraft velocity. This method is the basis of the sonic thermoanemometer. Such a method is barely influenced by velocity and humidity. These corresponding corrections can be easily calculated. Moreover, the temperature can be obtained at a very high frequency (100 Hz in our device) and without thermal lag. Compared with classical probes, the spatial resolution of our thermometer is increased by a factor about 100. At a speed of 100 m s^{-1}, our apparatus measures temperature every meter with resolution of 0.1°C.

2. Measuring method

The measuring method is a classical one and has already been successfully used in the case of ground-based instruments (Barrett and Suomi 1949; Schotland 1955; Gurvich 1959; Suomi and Businger 1959; Mitsuta 1966; Kaimal et al. 1968; Schotanus et al. 1983) and balloon-borne instruments (Ovarlez et al. 1978) intended for turbulence measurements. But until now, turbulence and the noise of the propellers precluded use of these systems from aircraft (Vinnichenko et al. 1967).

The adiabatic velocity of sound c_s in dry air is proportional to the square root of the temperature (Holton 1979, p. 155):

$$c_s = (\gamma_a R_a T)^{1/2} \tag{1}$$

where γ_a is the ratio between the specific heats C_{pa} and C_{va}, respectively at constant pressure and volume ($\gamma_a = C_{pa}/C_{va}$), and R_a is the specific gas constant: also, $R_a = R^*/M_a$ where $R^* = 8.31$ J mol^{-1} K^{-1} is the universal "perfect" gas constant, and M_a is the molecular weight of dry air. Thus, dry air temperature is obtained as a function of known constants and sound celerity.

Corresponding author address: Dr. D. Cruette, Laboratoire de Meteorologie, Universite Pierre et Marie Curie, 4, place Jussieu, Tour 15—25 E 5e, 75230 Paris Cedex 05, France.

Sound celerity may be easily measured in still air using a pair of transducers, one emitting, the other receiving. In the case of a relative airflow, we have to take into account the velocity V of the airflow. It then becomes necessary to use two emitter–receiver transducers in order to eliminate V: this is the well-known double-path method. Taking the example of two transducers 1 and 2 facing each other at a distance of L and set in an airflow directed from 1 to 2, the transit times from 1 to 2 and from 2 to 1 being, respectively, t_1 and t_2, we get for the relative velocities V_{12} and V_{21} between 1 and 2 (respectively, 2 and 1):

$$V_{12} = c_s + V = \frac{L}{t_1} \tag{2}$$

$$V_{21} = c_s - V = \frac{L}{t_2} \tag{3}$$

then

$$c_s = \frac{L}{2}\left(\frac{1}{t_1} + \frac{1}{t_2}\right) \tag{4}$$

and

$$V = \frac{L}{2}\left(\frac{1}{t_1} - \frac{1}{t_2}\right). \tag{5}$$

Hence, from t_1 and t_2 and knowing L, we obtain c_s from (4) and then the ambient temperature T from (1), it is also possible to obtain V from (5).

3. Adaptation to aircraft measurements

In the case of an airborne apparatus, we need to know three components of the relative velocity and then we must have three orthogonal measurement paths with, for each one, two pairs of emitter–receiver transducers.

In an early prototype we tried a triaxial measurement of V leading to the values of T, but problems inherent to the vibration of supports, reflections from supports, and interference between transducers led us to channel the airflow so as to be unidirectional.

a. Transducer choice and installation method

1) Choice of transducer

For environmental reasons (propeller noise for example) we chose transducers made from cylindrical piezoelectric ceramic elements with a resonance frequency of 100 kHz (length: 14 mm; diameter: 8 mm; piezoceramic P 160 manufactured by Quartz et Silice, France). In order to avoid interference between the nonpaired transducers, we selected emitters with a narrow radiation field.

2) Installation

This unidirectional device consists of a cylinder (length: 540 mm; diameter: 200 mm), the axis of which is placed in a parallel direction to the aircraft roll axis. Four transducers are situated in the horizontal plane through the cylinder axis (Fig. 1). They are located in the cylinder wall, in the corners of a square the length of which is the same as the cylinder diameter.

Writing the general equation of spherical wave propagation in a relative wind, the components of which are V_x, V_y, V_z, we obtain:

$$(x - V_x t)^2 + (y - V_y t)^2 + (z - V_z t)^2 = c_s^2 t^2. \tag{6}$$

Taking $V_z = V_y = 0$ and $V_x = V_0$, we obtain for t_1 (t_2), the transit time from E_1 to R_1 (E_2, R_2, respectively), the relations:

$$t_1 = \frac{L}{\sqrt{2}}\left[\left(2c_s^2 - V_0^2\right)^{1/2} - V_0\right]\left(c_s^2 - V_0^2\right)^{-1} \tag{7}$$

$$t_2 = \frac{L}{\sqrt{2}}\left[\left(2c_s^2 - V_0^2\right)^{1/2} + V_0\right]\left(c_s^2 - V_0^2\right)^{-1}. \tag{8}$$

Hence, from t_1 and t_2 we can obtain:

$$c_s = \frac{L}{\sqrt{2}}\left(\frac{1}{t_1^2} + \frac{1}{t_2^2}\right)^{1/2} \tag{9}$$

and

$$V_0 = \frac{L}{\sqrt{2}}\left(\frac{1}{t_1} - \frac{1}{t_2}\right), \tag{10}$$

and from c_s one deduces T [Eq. (1)].

b. Cylinder aerodynamics

Ultrasonic propagation is affected by turbulent phenomena. By reason of the cylinder wall thickness, turbulence appears in the flow. However, this turbulence can be reduced by a judicious choice of the leading and trailing edges of the cylinder.

1) Leading edge

Turbulence also may be induced by a possible yaw of the aircraft defined by the angle α between the relative velocity of the aircraft and its roll axis. We tried to define a leading edge allowing correct measurements up to yaw angles of $\pm 10°$.

We studied in a wind tunnel, for various profiles of the leading edge, the influence of yaw on turbulence. This was performed at the Institut d'Aérothermie (St. Cyr) and at the Laboratoire d'Aérodynamique (Ecole Nationale Supérieure des Arts et Métiers, Professor Driviere).

For four sections defined by their distance X from the entry of the cylinder (see Fig. 1), we measured with

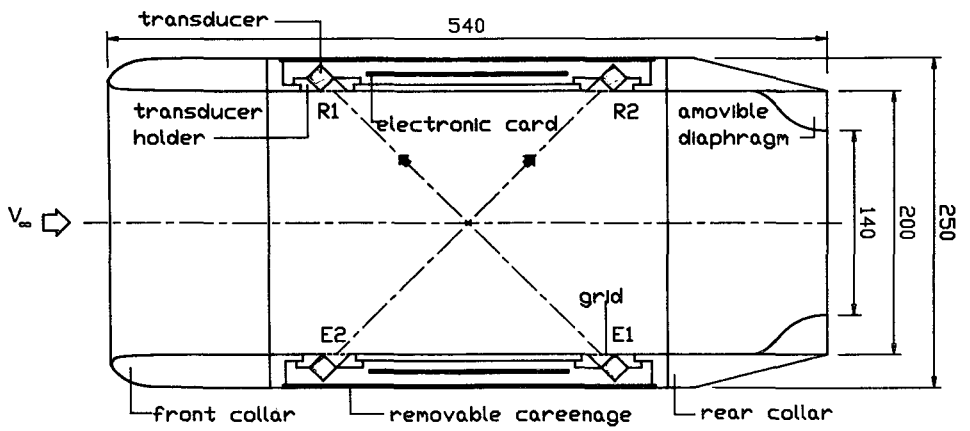

FIG. 1. Drawing of the sensor, front, and rear collars as described in the paragraph in section 3b. Here E_1 and E_2 are the emitters, and R_1 and R_2 the receivers.

a hot-wire anemometer the velocity V inside the cylinder, along a diameter. We plotted V/V_∞ as a function of the distance Y from the wall where V_∞ is the upstream velocity. Figure 2a shows the velocity profile measured in a cross section located midway between E_1–E_2 and R_1–R_2 (X = 280 mm with V_∞ = 50 m s^{-1} and $\alpha = 0°$. In this case a very thin leading edge was used for the purpose of reducing the thickness δ of the boundary layer, defined as the zone where V is less than $0.95V_\infty$. In symmetric conditions the boundary layer thickness is about 5 mm. Figure 9b shows velocity profiles for V_∞ = 50 m s^{-1}, $\alpha = +5°$, and X = 280 mm. We see that the yaw induces an asymmetry that increases the boundary layer thickness on the leeward side: δ varies from 2.5 mm on the windward side to 20 mm on the leeward side. This increase leads then to perturbation in the acoustic signal. By rounding the leading edge we improved the response of our device to the yaw: now the same velocity profile as in Fig. 2b is obtained for a larger value of the yaw ($\alpha = \pm 10°$).

2) TRAILING EDGE

In the previous experiment we observed in the wind tunnel that, for airspeeds larger than 50 m s^{-1}, the measurements became irregular due to fluctuations in signal amplitude. To correct this, we experimented with reducing the speed of the air in the cylinder by adding a removable diaphragm in the downstream extremity of the cylinder.

Let $\tau = \Delta A/A$ be the instability rate of the signal, where A is the amplitude of the received signal and ΔA is an estimate of its temporal fluctuation due to turbulence. We observed that for $\tau > 30\%$ the measurements become unusable.

Figure 3 shows the variation of τ as a function of the yaw angle for different values of diaphragm diameter.

It can be seen that

(i) for a given value of α (for example 10°), decreasing diameter values correspond to decreases in the signal instability, and

(ii) for a given value of τ (for example, 30%), it will be possible to reach greater yaw angle with smaller diaphragm diameter.

c. Corrections inherent to speed and to hygrometry

1) SPEED

A drawback of a diaphragm is that, due to energy conservation, the decrease in velocity inside the cylinder leads to an increase in inner temperature T_i.

Let T_e be the external temperature. Now $T_i - T_e = \Delta T$ may be calculated as follows. Using Bernouilli's law and in the case of an isentropic, nonviscous, compressible flow (velocity V, pressure P, density ρ), one obtains (Lamb 1959, p. 22)

$$\frac{V^2}{2} + \frac{dP}{\rho} = \frac{V^2}{2} + \frac{\gamma}{\gamma - 1}\frac{P}{\rho} = \text{constant} \qquad (11)$$

and then for a perfect gas ($\gamma = C_p/C_v$)

$$V_2 + 2C_pT = \text{constant}.$$

Hence, we obtain the so-called Barré de Saint-Venant's equation

$$\Delta T = T_i - T = V_i^2(2C_p)^{-1}\left(\frac{1}{\mu^2} - 1\right) \qquad (12)$$

or

$$\Delta T = V_e^2(2C_p)^{-1}(1 - \mu^2) \qquad (13)$$

where V_i = inner velocity, V_e = outer velocity

$$\mu = \frac{V_i}{V_e} \quad \text{and} \quad C_p = 1003 \text{ J K}^{-1} \text{ kg}^{-1}.$$

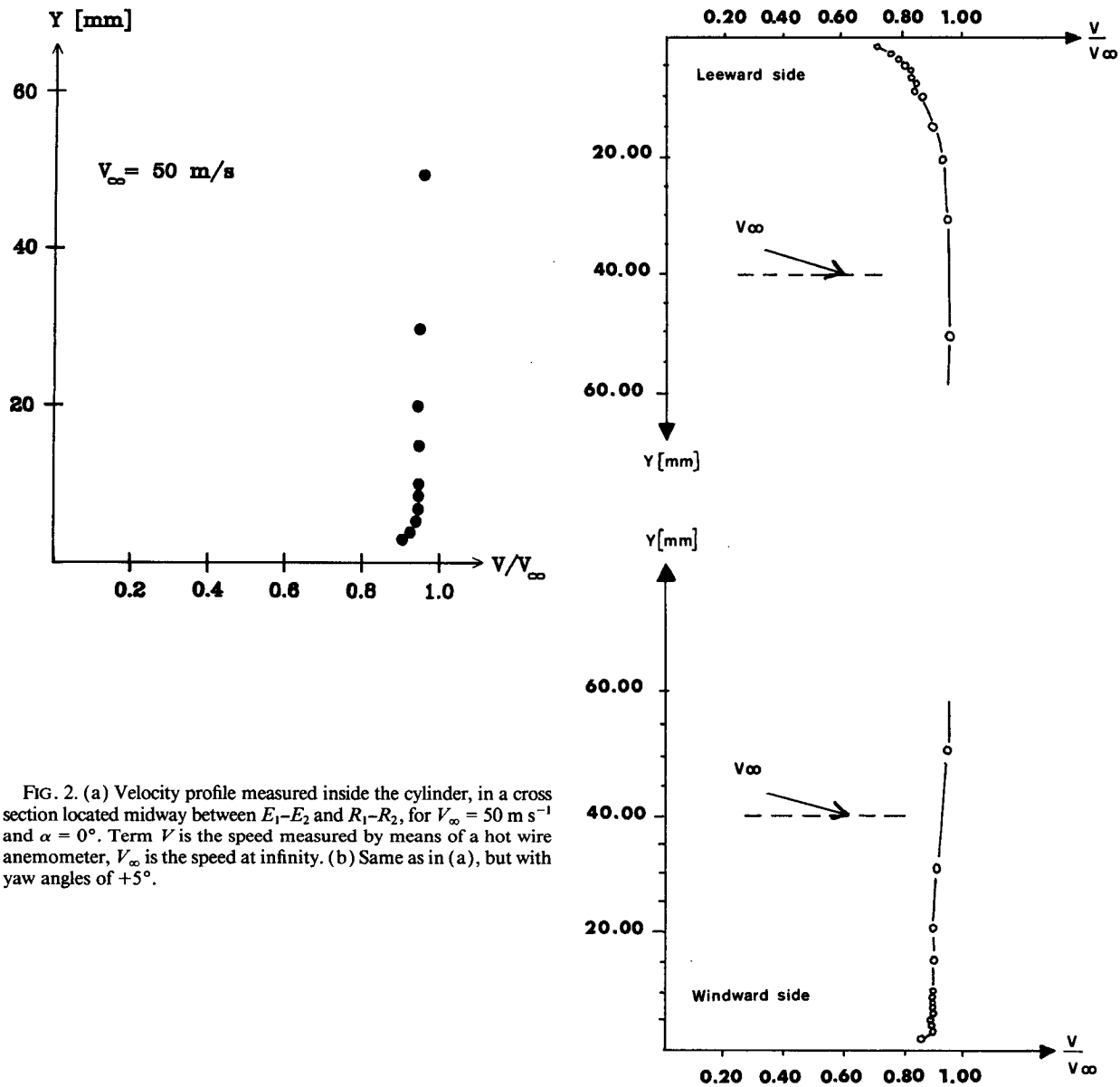

FIG. 2. (a) Velocity profile measured inside the cylinder, in a cross section located midway between E_1–E_2 and R_1–R_2, for $V_\infty = 50$ m s^{-1} and $\alpha = 0°$. Term V is the speed measured by means of a hot wire anemometer, V_∞ is the speed at infinity. (b) Same as in (a), but with yaw angles of +5°.

Here T_i and V_i are given by our device, and μ depends on the cylinder diaphragm diameters and has been measured in the wind tunnel. The value of μ is roughly proportional to the square of the diameters ratio (d_1 before the choke and d_2 at its level). For instance, for $d_1 = 196$ mm and $d_2 = 86.8$ mm: $\mu \approx 0.480$ up to 30 m s^{-1}. This correction is included in our software.

2) HUMIDITY

When the aircraft enters or leaves clouds, the relative humidity of the air inside the thermometer lies approximately between about 99% and 101% in cloudy air (Pruppacher 1978, p. 10) and 40% and 100% in clear air (CIAP 1975, 3–16). Since the thermodynamic constants that appear in Eq. (1) are affected by the hygrometric state of the air, the value of the measured temperature will be modified.

Let q be the specific humidity ($q \approx 0.622e/P; q \ll 1$) where e is the vapor pressure of water and P the total pressure of the air. Assuming that dry air and water vapor behave as perfect gases, one can calculate, using the generalized Dalton law (Queney 1974, p. 115), the thermodynamic constants for their mixture.

Thus, with R, C_v, and C_p being the gas constant and specific heats for humid air (R_a, C_{va}, C_{pa} for dry air; R_b, C_{vb}, C_{pb} for water vapor), one obtains

$$C_v = (1 - q)C_{va} + qC_{vb} = (1 + 0.93q)C_{va} \quad (14)$$

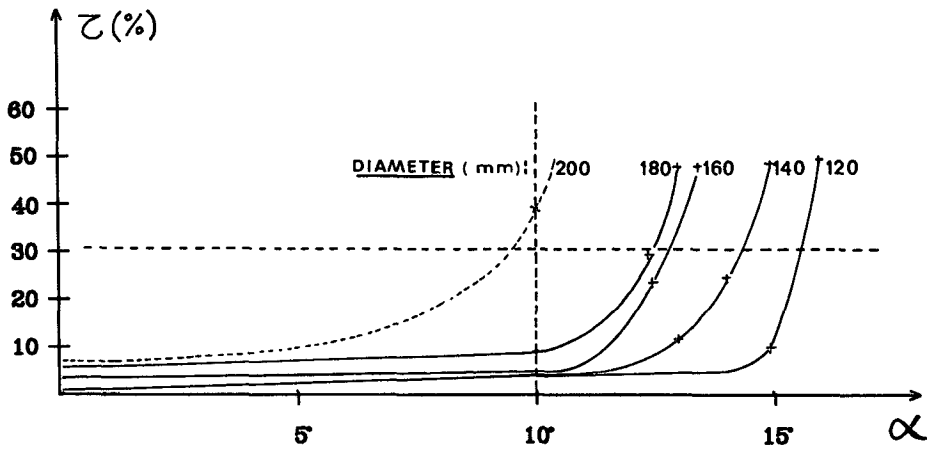

FIG. 3. Instability rate (τ) variation as a function of the yaw angle and for various diaphragm diameters. Here $\tau = \Delta A/A$ where A is the amplitude of the received signal and ΔA its fluctuations due to turbulence. For $\tau > 30\%$ the measurements become unusable.

and, in the same way

$$C_p = (1 + 0.84q)C_{pa} \tag{15}$$

$$R = (1 + 0.61q)R_a. \tag{16}$$

For $q \ll 1$ the true air temperature T' is then related to the temperature obtained from Eq. (1):

$$c_s = \gamma_a R_a T = \gamma R T' \tag{17}$$

$$T' = T\left(1 - 0.322\,\frac{e}{P}\right) = T(1 - 0.518q). \tag{18}$$

In the temperature range observed in real atmosphere, the correction due to humidity is about 3 K at ground level for saturated air and tends to decrease with altitude by reason of the mean decrease of T with altitude, and hence by the decrease of e.

d. Electronics

In order to obtain t_1 and t_2 (section 3a2), we have to perform very precise time interval measurements. Emitters are simultaneously excited by a high voltage burst (amplitude: 1500 V, duration: 50 μs) every hundredth of a second. The received signal is a pulse train of about ten cycles at 100 kHz (duration of this pulse: about 100 μs). The envelope of this train has a rise time of about 30 μs. The shape of the signal is presented in Fig. 4.

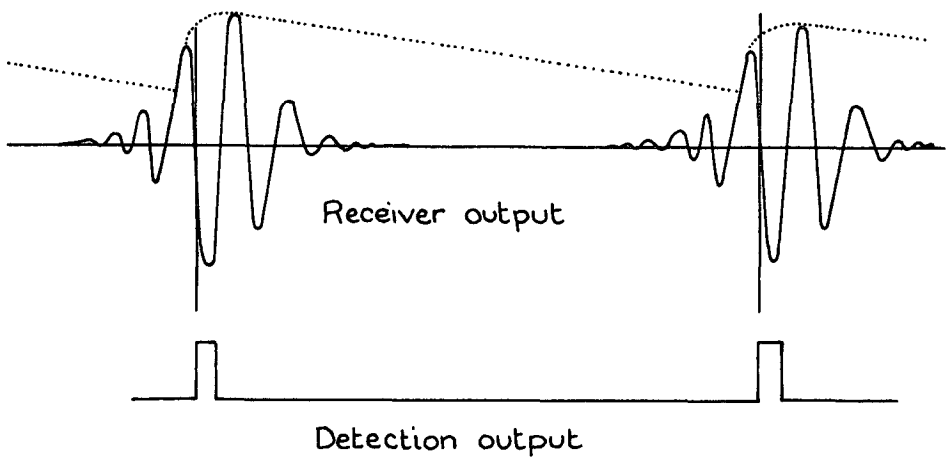

FIG. 4. Detection principle: the upper part of the figure represents two successive pulses, duration of a pulse is about 100 μs. The dotted line represents the peak detection of the signal, followed by a capacitive decrease. The intercept of this decrease with the following oscillating pulse defines the arch to be selected. The arrival time is then arbitrarily defined as the first crossing zero after the detection. The true arrival time is obtained by adding a calibration constant.

Because the received signal is oscillating inside the envelope it is difficult to define an "arrival time." We need then to identify a given point of this signal and measure the time interval between the start of the emitter pulse and this point. The true transit time will then be obtained by adding a calibration constant.

The reference time was selected as the first time the signal returns to zero after exceeding a specific threshold (Fig. 4). This method allows the best detection due to the large slope of the signal at this point. However, this method is only valid if one makes sure that the threshold always intercepts the same cycle of the signal (one cycle corresponds to a temperature change of about 3 K, and we know that the signal can present instabilities due to turbulence that prohibits any fixed electrical threshold. Thus, we choose a variable threshold, proportional to peak value of the preceding pulse. In this way, perturbations due to amplitude variations at a cadence lower than that of emission are avoided. Between the excitation and the zero-crossing time, clock pulses generated at a rate of 5 MHz are counted. This count is used as a measure of transit time for subsequent processing by a microcomputer. Figure 5 shows the block diagram of the apparatus.

4. Description of the instrument

The drawing of the sensor with or without the diaphragm is presented in Fig. 1. Figure 6 is a photograph of the final configuration of the instrument. The cylindrical part of the sensor holder is made from an aluminium alloy (AU 4 G). Stainless steel grids are placed in front of the transducers. The front and rear collars are formed from polypropylene.

The interior profile of the removable rear collar with diaphragm has been adjusted to avoid turbulent flow in the vicinity of the transducers.

Electronics are divided in three distinct parts, situated, respectively, between the two walls of the cylinder (A), in a control unit (B), and in one of the microcalculator slots (C) (Fig. 5 and Fig. 6). The control unit (B) contains power supplies and the synchronizing device. In the cylinder (A) are (Fig. 7) cards that produce the high voltage burst to be applied to the emitter and the reception cards that include the amplifier and the detecting devices. Furthermore, interface cards in both the control unit and the cylinder allow a numerical handshake between the sensor and the control unit.

The timer is placed on the microcalculator, which, by means of special software, allows us to obtain temperature and velocity in real time, to store files of calculated values, to obtain temperature versus time, to calculate mean values, and to display results. Connections between A and B are optical in order to avoid problems.

5. Preliminary aircraft tests

The cylinder was placed into a holding plate fixed to the wing undersurface. The aircraft was a Cessna 206 TU equipped with Rosemount (platinum probe, 100 Ω at 0°C) and reverse-flow (same as Rosemount but in special mounting designed by NCAR) probes for temperature measurements, and, for humidity, a dewpoint (Cambridge 137 C3) and a carbon (VIZ 11050 Ω at 33% RH) hygrometer. All these probes give one measurement per second.

Figure 8 shows the temperature recording of the ul-

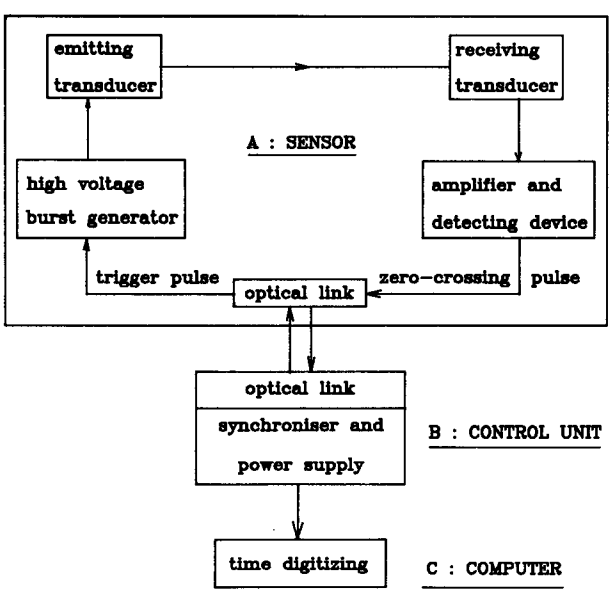

FIG. 5. Block diagram of the apparatus.

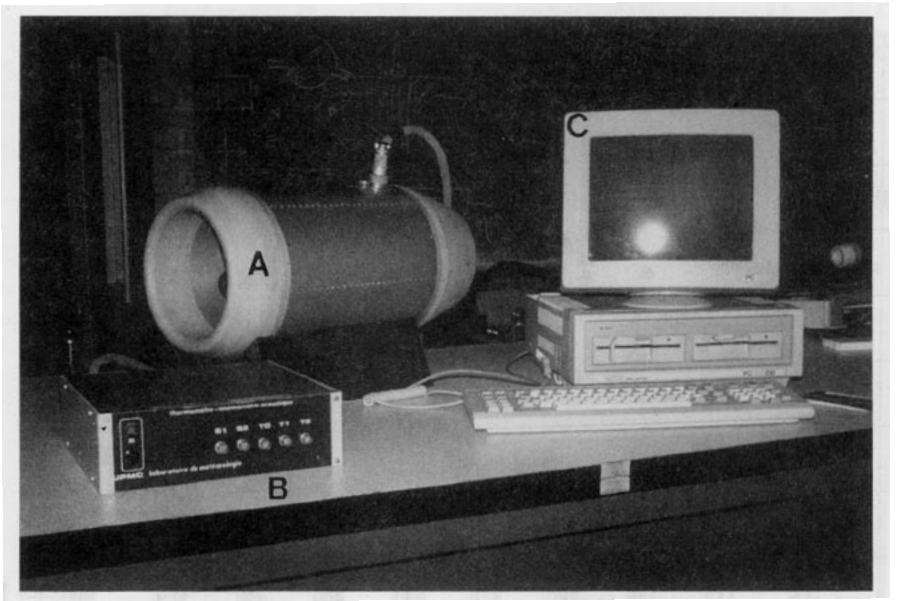

FIG. 6. Present configuration of the ultrasonic thermometer–anemometer: A—sensor holder; B—control unit; C—microcomputer.

trasonic thermometer, after humidity correction, during a horizontal flight compared with measurement obtained by means of the Rosemount and reverse-flow probes. Temperature values given by the ultrasonic thermometer are rounded by our program to the nearest 0.1 K, which explains the chopped shape of the recording. Notice that the measurement frequency of the Rosemount and the reverse flow used aboard the Cessna is 1 Hz, while our thermometer works at 100 Hz. We should say that both the Rosemount and the ultrasonic thermometer are in the same range of the temperature values. We can speculate on the discrepancy between reverse-flow and Rosemount probes: it seems that this is due to an incorrect functioning of

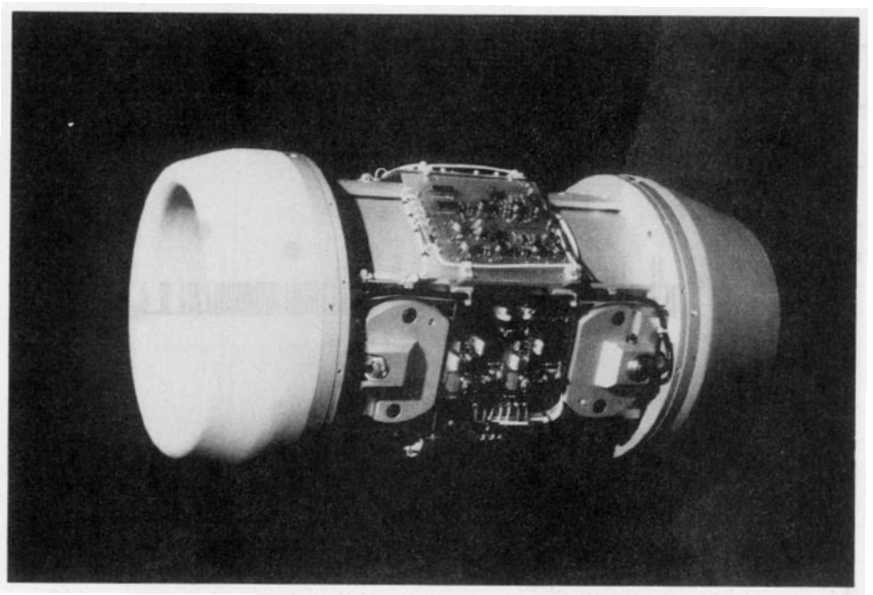

FIG. 7. The cylinder without its removable external walls. One can see two transducer holders and two of the electronic cards situated in the sensor. The front collar, with a rounded leading edge, is on the left of the photograph. The rear collar, with a thin trailing edge (but without diaphragm), is on the right.

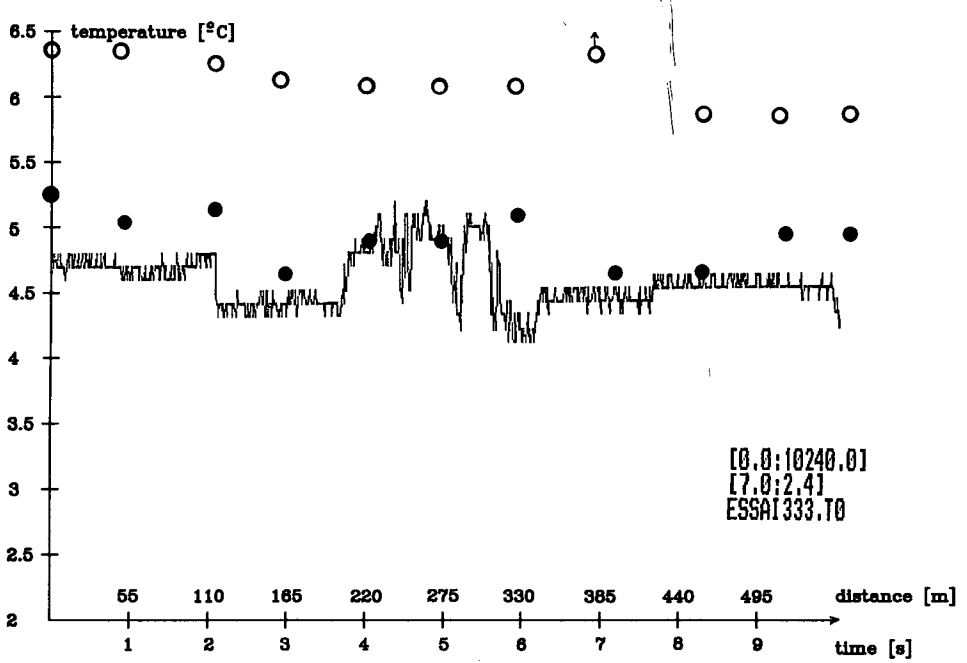

FIG. 8. Temperature recording of the ultrasonic thermometer, after humidity correction, during a horizontal flight at an altitude Z = 1500 m. Aircraft velocity: 55 m s^{-1}; yaw angle: 0°; humidity: 100%; nebulosity: fracto cumuli, 4/8. Open circles correspond to reverse flow probe measurements, black circles to Rosemount probe measurements. Temperature values are rounded by our software to the nearest 0.1 K, hence, the chopped shape of the recording.

reverse flow that has yet to be observed in this aircraft. We note that these measurements were obtained in a nonhomogeneous, cloudy environment (fracto cumuli). Given the spatial scale of the temperature variations, one can assume that there were true variations of air temperature.

Figure 9 shows temperature variations in clear air with an enlarged temperature scale. This recording

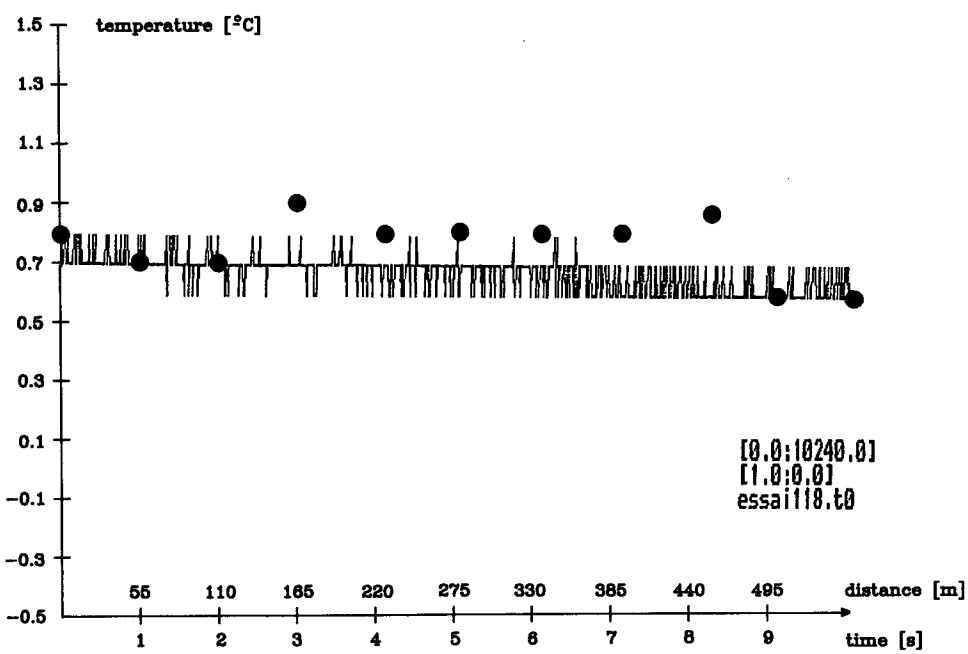

FIG. 9. Same as Fig. 8 with an enlarged scale for temperature and V = 55 m s^{-1}; yaw: 5°; humidity 72% (clear sky). This recording shows that a reasonable yaw does not disturb temperature measurements.

shows that a reasonable yaw does not disturb temperature measurements given by the ultrasonic thermometer.

Some measurements performed without the diaphragm for an aircraft of velocity $V = 55$ m s^{-1} have shown that the diaphragm was not necessary in these cases. Tests for airspeed higher than 55 m s^{-1} have not been possible because of the speed limit of the Cessna, but it seems likely that we will have to use the diaphragm.

6. Conclusion

This prototype of thermometer with a very fast response has worked in the usual speed range of the Cessna 206, that is, up to 200 km h^{-1}.

The next step is to couple this unit with a fast response hygrometer (100 Hz) in order to improve the humidity correction and to compare our instrument more extensively with an immersion thermometer under varying flight conditions and over a wide temperature range. Furthermore, this apparatus should be tested on a faster aircraft (Fokker 27) in order to determine the maximum speed at which it can operate.

Acknowledgments. This study was supported by DRET [Direction des Recherches Etudes et Techniques (Ministère des Armées)] and by the French Weather Bureau (Centre d'Aviation Météorologique) for flight tests. This prototype has been built in cooperation with the Laboratoire d'Aérodynamique de l'Ecole Nationale Supérieure des Arts et Métiers (Paris). We wish to thank all the students who have contributed to this study.

REFERENCES

Barret, E. W., and V. F. Suomi, 1949: Preliminary report on temperature measurements by sonic means. *J. Meteor.*, **6,** 273–276.

CIAP Monograph 4, 1975: *The natural and radiatiavely perturbed troposphere.* Department of Transportation, Climatic Assesment Program. National Technical Information Service, Springfield, Virginia.

Gurvich, A. S., 1959: Acoustic microanemometer for investigation of the microstructure of turbulency. *Acoustic J.* (USSR), **5,** 368–369.

Holton, J. R., 1979: *An introduction to dynamic meteorology.* Int. Geoph. series, Vol. 23. Academic Press, 391 pp.

Kaimal, J. C., and J. A. Businger, 1963: A continuous wave sonic anemometer thermometer. *J. Appl. Meteor.* **2,** 156–164.

——, J. C. Wyngaard and D. A. Haugen, 1968: Deriving power spectra from a three component sonic anemometer. *J. Appl. Meteor.*. **7,** 827–837.

Lawson, R. P. and W. A. Cooper, 1990: Performance of some airborne thermometers in clouds. *J. Atmos. Ocean. Technol.*, **7,** 480–494.

Lamb, Sir H., 1959: *Hydrodynamics,* Cambridge University Press, 737 pp.

Mitsuta, Y., 1966: Sonic anemometer–thermometer for general use. *J. Meteor. Res. Japan,* **44,** 12–23.

Ovarlez, J., H. C. Cabrita, D. Cadet and H. Ovarlez, 1978: A balloon-borne sonic anemometer–thermometer. *Fourth Symp.* on *Meteorological Observations and Instrumentations,* Denver, Amer. Meteor. Soc., 65–68.

Pruppacher, H. R., and J. D. Klett, 1978: *Microphysics of clouds and precipitations.* D. Reidel, 714 pp.

Queney, P., 1974: *Eléments de Météorologie,* Masson et Cie, 300 pp.

Schotanus, P., F. T. M. Nieuwstadt, and H. A. R. De Bruin, 1983: Temperature measurements with a sonic anemometer and its application to heat and moisture flure. *Bound. Layer. Meteor.*, **26,** 81–93.

Schotland, R. M., 1955: Measurement of wind velocity by sonic means. *J. Meteor.*, **12,** 386–390.

Suomi, V. E., and J. A. Businger, 1959. *Principle of the sonic anemometer–thermometer. AFCRC-TR-58-235* Geophys. Res. Papers No. 59, 673 pp.

Vinnichenko, N. K., N. Z. Pinus, S. M. Shmeter, and G. N. Shur, 1973: *Turbulence in free atmosphere.* Plenum, 263 pp.